Available online at www.sciencedirect.com
ScienceDirect
Biochimica et Biophysica Acta 1767 (2007) 178–188
Biochimica et Biophysica Acta
BBA
www.elsevier.com/locate/bbabio

Functional properties of type I and type II cytochromes c_3 from *Desulfovibrio africanus*

Catarina M. Paquete [a,1], Patrícia M. Pereira [a,1], Teresa Catarino [a,b,*], David. L. Turner [a,c], Ricardo O. Louro [a], António V. Xavier [a,†]

[a] *Instituto de Tecnologia Química e Biológica, Universidade Nova de Lisboa, Rua da Quinta Grande, 6, Apt. 127, 2780-156 Oeiras, Portugal*
[b] *Departamento de Química, Faculdade de Ciências e Tecnologia, Universidade Nova de Lisboa, Quinta da Torre, 2829-516 Caparica, Portugal*
[c] *School of Chemistry, University of Southampton, Southampton SO17 1BJ, UK*

Received 9 November 2006; received in revised form 9 January 2007; accepted 17 January 2007
Available online 25 January 2007

Abstract

Type I cytochrome c_3 is a key protein in the bioenergetic metabolism of *Desulfovibrio* spp., mediating electron transfer between periplasmic hydrogenase and multihaem cytochromes associated with membrane bound complexes, such as type II cytochrome c_3. This work presents the NMR assignment of the haem substituents in type I cytochrome c_3 isolated from *Desulfovibrio africanus* and the thermodynamic and kinetic characterisation of type I and type II cytochromes c_3 belonging to the same organism. It is shown that the redox properties of the two proteins allow electrons to be transferred between them in the physiologically relevant direction with the release of energised protons close to the membrane where they can be used by the ATP synthase.

Keywords: Cytochrome c3; Desulfovibrio africanus; Electron transfer rates; Multicentre protein; Thermodynamic characterisation

1. Introduction

Sulphate reducing bacteria (SRB) are metabolically versatile organisms with the ability to use multiple respiratory substrates, such as hydrogen or organic compounds, giving rise to hydrogen sulphide as the end-product of sulphate reduction [1]. They are widespread in anaerobic environments and their participation in biocorrosion and souring of oil and gas deposits has attracted considerable attention from the oil industry [2,3]. There is evidence suggesting that they may be implicated in inflammatory bowel diseases of humans [4], and these bacteria may also have environmental applications in bioremediation processes [5].

Desulfovibrio (*D.*) is the best studied genus of SRB. The genome of *Desulfovibrio vulgaris* Hildenborough has been fully sequenced, showing the presence of at least 14 multihaem cytochromes *c* involved in the respiratory electron transfer pathways [6]. Type I tetrahaem cytochrome c_3 (TpIc_3) is the most abundant periplasmic protein, reaching up to 30% of the total [7], and it is the best characterised of the electron transfer proteins with respect to its structure–function relationship [8]. TpIc_3 is a small (13.5–15 kDa) soluble protein that contains four *c*-type haems with bis-histidinyl axial coordination, which are covalently bound to the polypeptide chain through thioether bonds. Although the TpIc_3 from different organisms present low sequence homology, they share a conserved three dimensional fold as well as a conserved arrangement of the four haem groups [9]. All four haems have negative reduction potentials and their close proximity results in homotropic redox cooperativity. Microscopic reduction potentials are pH dependent in the physiological pH range (redox-Bohr effect) [10–12] which is evidence of thermodynamic coupling of the transfer of electrons and protons [13]. TpIc_3 mediates the transfer of electrons from hydrogenase to membrane-bound redox complexes [14–19] and

Abbreviations: SRB, Sulphate reducing bacteria; TpIc_3, Type I cytochrome c_3; TpIIc_3, Type II cytochrome c_3; *D.*, *Desulfovibrio*; *Dsm.*, *Desulfomicrobium*; NMR, Nuclear Magnetic Resonance

* Corresponding author. Instituto de Tecnologia Química e Biológica, Universidade Nova de Lisboa, Rua da Quinta Grande, 6, Apt. 127, 2780-156 Oeiras, Portugal. Fax: +351 21 4428766.
E-mail address: catarino@itqb.unl.pt (T. Catarino).
† Deceased 7th May 2006.
[1] Contributed equally to the work.

0005-2728/$ - see front matter © 2007 Elsevier B.V. All rights reserved.
doi:10.1016/j.bbabio.2007.01.012

enhances the activity of the periplasmic hydrogenase at physiological pH [20]. The energy transduction that arises from the coupled affinity for electrons and protons lowers the pK_a of the protons and contributes to acidifying the periplasmic space, which facilitates ATP synthesis [20,21].

Of the multihaem cytochromes that are downstream partners of TpIc_3, TpIIc_3 has been studied in most detail [22,23]. TpIIc_3 was identified as part of a polycistronic operon that encodes for a transmembrane electron transfer complex designated Tmc [16,19]. Furthermore, although the comparison of the crystal structures of these two types of cytochromes c_3 [23,24] shows that the architecture of the four-haem cluster and the overall protein fold is similar, TpIIc_3 displays localised differences: haem I is more exposed to the solvent and is surrounded by a negative surface region, and haem IV lacks the typical lysine patch [16,24]. When compared with TpIc_3, TpIIc_3 presents poor reactivity with hydrogenases [16,25], suggesting that it is not a physiological partner of these enzymes. However, the presence of catalytic amounts of TpIc_3 increases the reactivity of TpIIc_3 towards hydrogenase, which indicates an interaction between the two cytochromes. Docking studies between TpIc_3 and TpIIc_3 showed that there are possible interactions between the two proteins but a clear picture does not emerge because the TpIc_3/TpIIc_3 complex has been reported to present different stoichiometry for the species *D. vulgaris* Hildenborough and *Desulfovibrio africanus* [23].

Theoretical studies indicate that complex formation induces changes in the reduction potentials of both cytochromes, allowing the flow of electrons [26]. However no detailed experimental study of the redox properties of TpIc_3 and TpIIc_3 isolated from the same organism has been published so far. In this work, we report the thermodynamic and kinetic characterisation of TpIc_3 and TpIIc_3 isolated from *D. africanus*.

2. Materials and methods

2.1. Protein purification

D. africanus, strain Benghazi (NCBI 8401) was grown anaerobically at pH 7.2 as previously described [25]. All purification steps were performed at pH 7.6 and 4 °C in a FPLC system (Pharmacia). Cytochromes were purified from *D. africanus* soluble fraction as previously described for TpIc_3 [25] and TpIIc_3 [22].

2.2. Preparation of NMR sample of TpIc_3

The NMR samples were prepared in ^2H_2O as described in [27] with a final concentration of 5–6 mM. The NMR experiments of partially oxidised samples were performed with a final concentration of 1–2 mM in order to obtain conditions of slow intermolecular electron exchange. The ionic strength was set to 50 mM or 100 mM by addition of KCl. The pH was adjusted by addition of small amounts of ^{2}HCl or NaO^{2}H and measured inside an anaerobic chamber to avoid sample re-oxidation in the case of reduced and partially oxidised samples. The pH values reported in this work are not corrected for the isotope effect. Catalytic amounts of *Desulfovibrio gigas* [NiFe] and *D. vulgaris* Hildenborough [Fe] hydrogenases were added to the sample in a hydrogen atmosphere to reduce the cytochrome.

2.3. NMR experiments with TpIc_3

All ^{1}H NMR spectra were obtained in a 500-MHz Bruker DRX spectrometer equipped with an inverse detection 5 mm probe head and a Eurotherm 818 temperature control unit.

Chemical shifts are reported relative to DSS and spectra were calibrated using the residual water signal as an internal reference [28].

Processing of all NMR data and measurement of the signal positions and linewidths in the partially oxidised samples was performed using standard Bruker software. The assignment of signals in the reduced and oxidised states was performed using the CARA program [29].

2.3.1. NMR experiments of the reduced state

NOESY spectra were acquired with mixing times of 50 and 200 ms and TOCSY spectra were performed with 40 and 60 ms spin-lock times. A selective pulse of 500 ms was used for water presaturation. The experiments were recorded at 300 and 310 K and at pH 8.2 using a spectral width of 35 kHz.

2.3.2. NMR experiments of partially oxidised samples

To establish the complete pattern of oxidation for each haem methyl group at each pH, several 2D-exchange spectroscopy (EXSY) NMR data sets, with 25 ms of mixing time, were collected at 298 K. Experiments in intermediate states of oxidation were performed in a pH range spanning 8.8 to 5.2. 2D-ROESY experiments were performed with a spin-lock field of 10 kHz at 298 K and at three different pH values (pH 8.4, 7.6, 6.4) to distinguish unequivocally nOe cross peaks from exchange cross peaks.

2.3.3. NMR experiments of the oxidised state

The experiments in the fully oxidised state were performed at 295 and 300 K and at pH 5.4. NOESY experiments were performed with 25 and 75 ms mixing times and the TOCSY experiment with 60 ms spin-lock time. A double quantum filtered COSY was also collected. All experiments were prepared using a selective pulse of 500 ms to saturate the residual water signal.

The ^{1}H–^{13}C HMQC experiments were collected with ^{13}C decoupling during acquisition at 285, 295 and 300 K.

2.4. Redox titrations followed by visible spectroscopy

Redox titrations of the TpIc_3 and TpIIc_3 followed by visible spectroscopy were performed at 298.0±1.0 K as described in the literature [30]. TpIc_3 was prepared in 100 mM Tris/maleate buffer at pH 6.6 and pH 8.1, whereas TpIIc_3 was prepared in 100 mM Tris/maleate buffer at pH 6.4 and pH 7.9. Both protein solutions were prepared inside an anaerobic chamber (Mbraun MB150-GI). A cocktail of redox mediators was prepared according to the recommendations in the literature [31]. Methyl viologen, neutral red, diquat, safranine O, anthraquinone 2,7-disulfonate, anthraquinone 2-sulfonate, indigo tetrasulfonate, indigo disulfonate and indigo trisulfonate were used for all experiments. This mixture was supplemented with phenosafranine at pH 6.6 and pH 6.4, and with methylene blue and gallocyanine at pH 8.1 and pH 7.9. In order to guarantee the absence of interactions between the redox mediators and the protein, different concentration ratios of protein vs. mediators were tested. The data presented here was obtained with a protein concentration of ca. 20 μM and the concentration of each mediator was 1–1.5 μM.

2.5. Kinetic studies

2.5.1. Sample preparation

Tris/maleate buffer in the pH range 5.5–8.5 with a concentration of 100 mM after mixing was prepared inside an anaerobic chamber (M-Braun MB150) with degassed water. Stock solutions of TpIc_3 and TpIIc_3 were degassed with cycles of argon gas and vacuum in order to remove the dissolved oxygen. The concentration of the protein was determined after each kinetic experiment by UV-visible spectroscopy using ε_{552}=120 000 M^{-1} cm^{-1} for the reduced protein, and the actual pH of the reaction was measured after each experiment.

Sodium dithionite was recrystallised as described in [30] in order to obtain >95% pure material and used as the reducing agent. Solid sodium dithionite was added to degassed Tris/maleate buffer 5 mM at pH 8.5 inside the anaerobic chamber to give the approximate desired concentration. For each experiment the actual concentration of the reducing agent was measured, inside an anaerobic chamber, by UV-visible spectroscopy using ε_{314}=8000 M^{-1} cm^{-1} [32]. The ionic strength of this buffer was set to 100 mM by addition of KCl.

To perform rapid mixing kinetic experiments starting with various degrees of reduction of the protein sample, a few microliters of concentrated sodium dithionite solution were added to the protein solution before running the experiments.

2.5.2. Data collection

Rapid mixing kinetic experiments were carried out in a HI-TECH Scientific SF-61 stopped-flow instrument installed inside an anaerobic chamber where the oxygen level was kept below 0.2 ppm. The data were acquired at 552 nm with a large excess of dithionite (~100:1) to ensure essentially irreversible pseudo first order kinetics as previously described [30].

2.6. Thermodynamic and kinetic modelling

The data from redox titrations followed by NMR and by visible spectroscopy and from kinetic experiments were fitted simultaneously to a thermodynamic model [11] and to a kinetic model [33] as described in the literature [30]. These models consider five charged centres interacting with each other, which correspond to the four haems and one acid base group. The NMR data only defines the relative redox potentials and interactions of the haems and the absolute haem–proton interactions. Visible redox titrations provide a calibration of the haem potentials and the haem–haem interactions. According to the kinetic model, the shape and pH dependence of the kinetic traces also contain information about the thermodynamic parameters of the redox centres via the driving force for electron transfer and the populations of the microstates. Fitting the kinetic traces as well as the NMR data and visible titrations requires four additional parameters [33]. In model 1, these are a reference rate constant for each haem, which is related to structural factors such as accessibility for the reducing agent. In model 2, the four parameters are ascribed to the four consecutive one-electron steps and the environments of the four haems are indistinguishable. Although each trace would yield at most two parameters, the complete set of pH dependent traces together with the experiments with partially reduced samples is sufficient to define the four kinetic parameters.

3. Results

3.1. Protein purification of TpIc$_3$

The yield of *D. africanus* TpIc_3 was ca. 30 mg/kg wet cell paste and the purified protein displayed UV-visible spectra in agreement with the results reported in the literature [25].

3.2. Resonance assignment of TpIc$_3$ in the reduced protein

The assignment of the haem NMR resonances of the TpIc_3 in the reduced form was performed using a strategy adapted from that previously described [34]. The specific and self-consistent assignment for the resonances of the four haems is listed in Table 1. Interhaem connectivities in the NOESY spectra for closely spaced substituents of different haems further confirmed the assignment. The ring current shifts which arise from the haems and aromatic residues were calculated as previously described [35] using the coordinates from the crystal structure 2BQ4 [23] and are in good agreement with the experimental data (Fig. 1), indicating that there is a close similarity between the crystal and the solution structure.

3.3. Resonance assignment of TpIc$_3$ in the oxidised protein

2D EXSY and 2D ROESY experiments allowed the classification of twelve of the sixteen haem methyls into four sets according to the pattern of oxidation observed in those experiments. Data were collected at two temperatures in order to resolve ambiguities in the assignment resulting from closely placed signals. The haem methyl groups M2^1 I and M2^1 III (nomenclature according the IUPAC-IUB recommendations [36] and Roman numbers indicate the order of the haem attachment to the polypeptide chain) were assigned from intrahaem cross-peaks. The two remaining methyl signals, M7^1 I and M12^1 II, were assigned on the basis of the expected symmetry of the shifts at the periphery of the haem. Haem III was readily assigned to the structure due to the characteristic pattern of the shifts for the haem substituents with a very large paramagnetic shift for the α protons of propionate 13 and a very small shift for the M18^1. Haem IV was identified on the basis of the observation of the M2^1 III–M12^1 IV interhaem signal, typical of cytochromes c_3 [13,37–39]. The signal M2^1 III–M12^1 I was not observed with a 75 ms mixing time and therefore the structural assignment of the signals of haems I and II has to rely on the relationship between the pattern of the shifts and the structure. Fortunately, the geometry of the axial ligands of haem II is closely similar in both molecules A and B in the unit cell [23], so the uncertainty is small and the assignment can be made unambiguously. The assignments of the proton and carbon signals of the haem substituents in the oxidised state of the cytochrome are listed in Table 2. A few nuclei are expected to have small paramagnetic shifts, either in ^{13}C or in ^{1}H frequency, and their signals could not be confidently assigned in the protein envelope.

Table 1
Proton chemical shifts of haem substituents in reduced *D. africanus* TpIc_3, at pH 8.2 and 310 K and 50 mM ionic strength

Haem substituent[a]	Chemical shifts of haem protons (ppm)			
	Haem I	Haem II	Haem III	Haem IV
5	10.15	8.92	9.40	8.99
10	9.91	8.82	9.02	9.60
15	9.81	9.59	9.02	9.76
20	10.24	9.69	9.11	9.45
2^1	4.51	4.00	4.34	4.35
7^1	3.97	3.32	3.42	2.84
12^1	3.59	3.18	3.25	3.15
18^1	3.66	3.28	3.93	3.15
3^1	7.11	5.74	5.68	6.26
8^1	6.52	4.76	5.81	6.05
3^2	2.19	0.45	2.02	2.36
8^2	3.02	0.42	1.89	1.34

[a] The IUPAC-IUB nomenclature is used for the haem ring substituents.

3.4. Structural characterisation of the haem coordination environment

A model of the haem molecular orbitals [40] was fit to the ^{13}C NMR data of the substituents at the periphery of the haems measured at 300 and 285 K. According to this model the frontier molecular orbitals of the haem are characterised by two parameters, a rhombic perturbation and the energy splitting which are dominated by the orientation of the axial ligands. On this basis, the orientation of the axial histidines planes can be determined from NMR data with a similar confidence to that

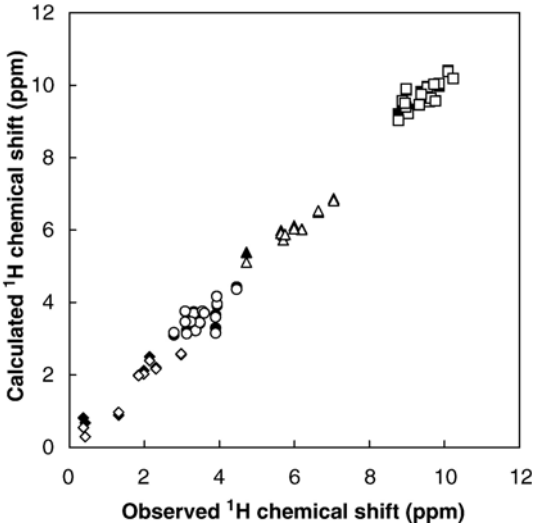

Fig. 1. Calculated versus observed chemical shifts for the haem substituents of reduced *D. africanus* TpIc$_3$. The ring current shifts were calculated as in [35] using molecules A (solid symbols) and B (open symbols) of the crystal structure: methyls (○); meso protons (□); thioether methines (Δ); and thioether methyls (◊).

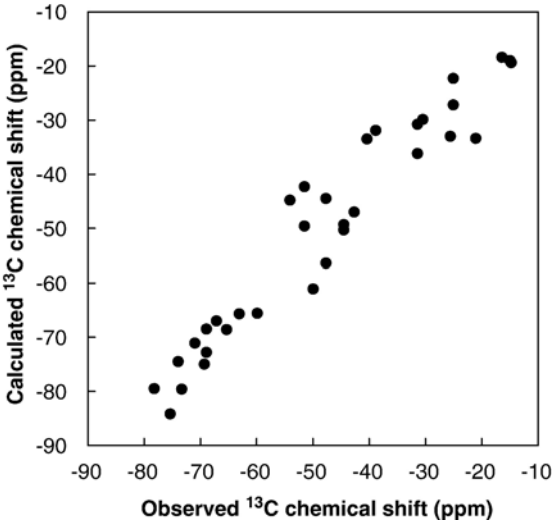

Fig. 2. Calculated versus observed ^{13}C chemical shifts for the haem substituents of oxidised *D. africanus* TpIc$_3$. The chemical shifts for the haem substituents were calculated as described in [40].

expected from X-ray diffraction. These results are shown in Fig. 2 and Table 3.

3.5. Thermodynamic and kinetic characterisation

Intermolecular electron exchange is slow in the NMR timescale under the conditions used for the NMR experiments. In these conditions each haem substituent displays five discrete NMR signals that correspond to each of the five redox stages connected by four steps of a single electron transfer [12]. Because the paramagnetic shift is proportional to the degree of oxidation of the haems, in each stage the chemical shift of the haem substituent depends on the relative oxidised fraction of that haem. The position and the linewidth of the resonance of one methyl group belonging to each haem of TpIc_3 were measured in the samples poised at various levels of reduction. Methyls 18^1 for haem I, II and IV and 12^1 for haem III were selected because they constitute the best compromise between a considerable paramagnetic shift and orientation towards the protein surface to minimize extrinsic paramagnetic effects caused by neighbouring haems. These extrinsic shifts were accounted for using the methods described in the literature [37]. The NMR data used for the characterisation of TpIIc_3 were those previously published [22], but with a new set of visible redox titrations, where the possibility of interactions between the cytochrome and the redox mediators was eliminated.

The simultaneous fit of the thermodynamic and kinetic models to the experimental data did not change significantly the values of the thermodynamic parameters obtained from the fitting of the thermodynamic data alone. However, the quality of the fit with model 1 was significantly better than that with model 2, as might be expected given the different environments of the four haems, and the results from model 1 are presented in Figs. 3–5, with the optimised thermodynamic parameters for TpIc_3

Table 2
Chemical shifts of haem resonances in *D. africanus* TpI ferricytochrome c_3, at pH 5.4 and 300 K

Haem Substituent[a]	Haem I		Haem II		Haem III		Haem IV	
	^{13}C	^{1}H	^{13}C	^{1}H	^{13}C	^{1}H	^{13}C	^{1}H
2^1	−52.68	22.17	−19.03	5.11	−22.06	3.42	−31.4	9.74
3^1	n.d.	n.d.	n.d.	n.d.	−42.90[b]	2.27	n.d.	n.d.
3^2	n.d.	n.d.	n.d.	n.d.	n.d.	n.d.	n.d.	n.d.
7^1	−9.26	4.58	−29.30	19.65	−52.62	22.40	−43.38	20.65
8^1	n.d.	n.d.	n.d.	n.d.	n.d.	n.d.	−50.74[b]	3.65
8^2	n.d.	n.d.	n.d.	n.d.	n.d.	n.d.	n.d.	n.d.
12^1	−55.58	19.00	−18.93	7.21	−16.91	9.62	−30.4	11.8
13^1	6.63	−0.62	n.d.	n.d.	−59.16	18.51	8.37	−0.26
		−1.27				17.27		−4.56
17^1	−2.20	2.14	−24.63	5.29	n.d.	n.d.	−19.50	9.47
		4.22		6.78				8.67
18^1	−61.49	27.51	−54.02	27.68	−5.95	1.08	−62.00	31.39

[a] The IUPAC-IUB nomenclature is used for the haem substituents.
[b] Tentative assignments.

Table 3
Electronic structure parameters of the frontier molecular orbitals of the haems in *D. africanus* TpIc_3 determined from ^{13}C NMR data, at 285 and 300 K and from X-ray structure

	^{13}C NMR data			X-ray structure			
				Molecule A		Molecule B	
	ΔE (kJ/mol)	θ (°)	β (°)	θ (°)	β (°)	θ (°)	β (°)
Haem I	−4.1	−38	0	−25	16	−61	16
Haem II	−3.3	−11	55	−21	42	−7	47
Haem III	−4.1	57	19	61	21	58	7
Haem IV	−3.4	−15	52	−3	39	−23	67

The absolute value of ΔE can be related with the acute angle between the axial ligand planes, β, and the orientation of the bisector, θ, according to the empirical equation $\Delta E = (5 + \cos 4\theta) \cos \beta$. The value of Qcc was fixed at −36 MHz [39].

and TpIIc_3 reported in Table 4. The diagonal terms are the free energies necessary to oxidise the four haems and to deprotonate the acid/base centre, while the off-diagonal terms are the interaction energies between each pair of haems (homotropic cooperativities) and the interactions between the haems and the acid/base centre (heterotropic cooperativities). These energies are reported in units of millielectron volt and therefore the diagonal values are numerically equal to the reduction potentials. In TpIc_3, the large separation between the reduction potential of haem III and the other three haems prevents the determination of its haem–haem interaction energies, which are implicitly included in the value of the diagonal term. Thus the free energy of oxidation of haem III can only be evaluated for the situation where the other three haems are already oxidised. A similar situation has already been encountered for TpIc_3 from *Desulfomicrobium* (*Dsm.*) *norvegicum* and *Dsm. baculatum* [30,41]. Although NMR and kinetic data do not provide experimental information to define the electron–proton interactions affecting this haem, the redox titrations followed by visible spectroscopy show that this haem is subject only to a very small interaction in the pH range studied.

In the case of TpIc_3, the energy for the interaction of the acid–base centre with the haems is larger for haem I as observed for other TpIc_3 [11,30,37,42]. For a few cases the propionate 13 of haem I was identified as the responsible residue [11,21,30,37,38,42] but in the present data the interaction is weaker.

NMR and electrochemical methods have shown that the macroscopic and microscopic redox potentials can be affected by the ionic strength [43]. Comparison of the data obtained at 50 mM KCl (data not shown) and data obtained at 100 mM KCl for TpIc_3 shows little change between the two conditions, with values differing by more than 10 meV only found for the oxidation energy of haem III and for its interaction with the acid–base centre. Because the parameters associated with haem III are the least well defined, the significance of these differences is small.

Table 5 reports the macroscopic pK_a values associated with each macroscopic oxidation stage (numbered 0–4 according of the number of oxidised haems) for TpIc_3 and TpIIc_3 showing that the pK_a values span the physiological range in both cases.

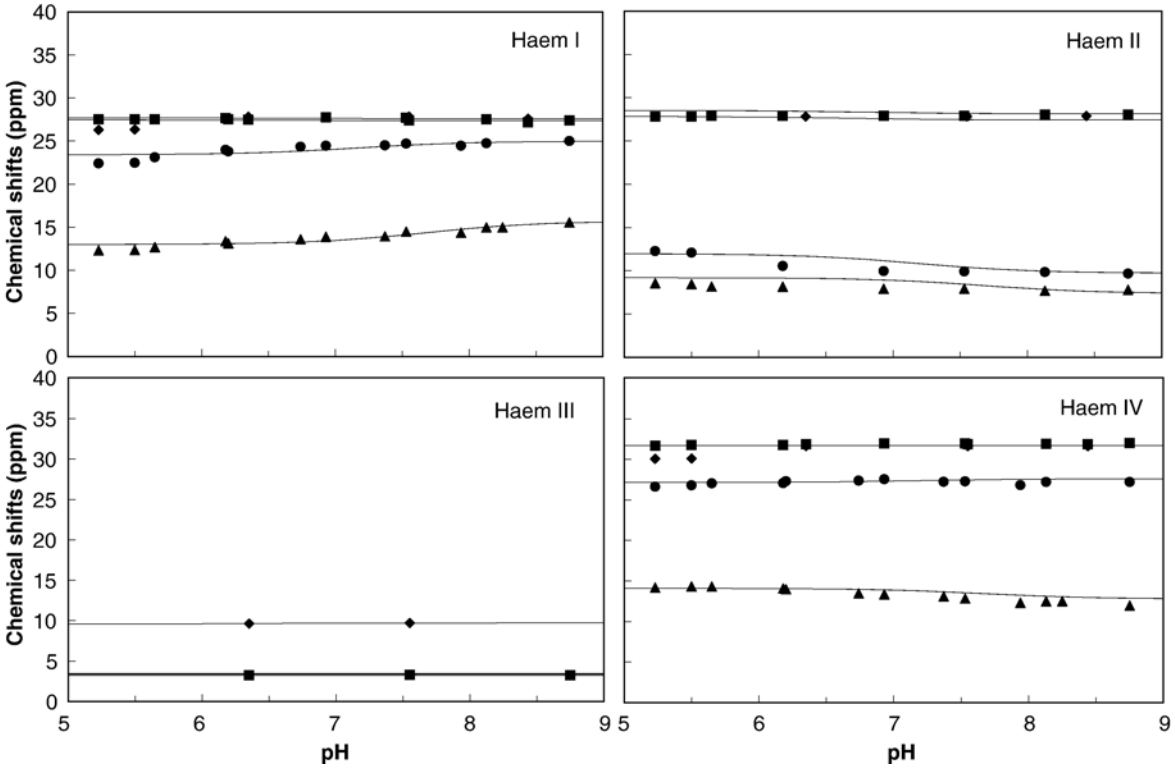

Fig. 3. pH dependence of the ^{1}H NMR chemical shifts of one methyl group from each of the four haems of *D. africanus* TpIc_3 in different stages of oxidation. Stages of oxidation 1–4 are represented by the symbols: stage 1 (Δ); stage 2 (○); stage 3 (□) and stage 4 (◊). The full lines represent the best fit of the data using the parameters reported in Table 4.

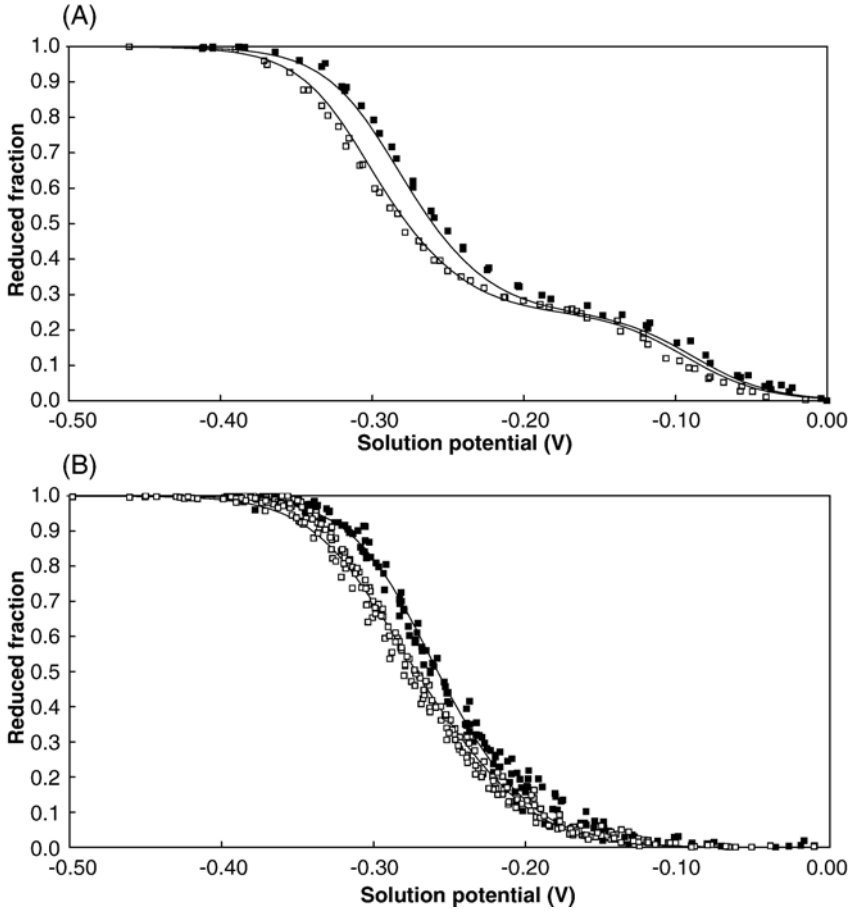

Fig. 4. Visible redox titrations performed at 298 K for *D. africanus* TpIc_3 and TpIIc_3. (A) TpIc_3 at pH 6.6 (filled symbols) and pH 8.1 (open symbols). (B) TpIIc_3 at pH 6.4 (filled symbols) and pH 7.9 (open symbols). The solid lines represent the best fit of the experimental data using the parameters reported in Table 4.

Fig. 5 shows the kinetic data obtained for the reduction of the two cytochromes with sodium dithionite at different pH values and the fitted curves obtained with the kinetic model, with the thermodynamic parameters reported in Table 4 and the reference rate constants reported in Table 6. The reference rate constants, k_i^0, are assigned to each individual haem according to model 1 [33] and include structural factors such as solvent exposure. The fitted curves show excellent agreement with the kinetic data obtained for TpIc_3 and TpIIc_3. The simultaneous fit of the thermodynamic and kinetic data also allows a better definition of the thermodynamic parameters, especially those related with the redox-Bohr effect, because of the rate dependence with pH that is observed in the vicinity of the pK_a of the redox-Bohr group. For example, the kinetic data for TpIIc_3 show little change between pH 7.3 and pH 8.5 because the pK_a is below 7 in every stage except the fully oxidised protein (see Table 5), which is not clear from the visible titrations or from the NMR data at the pH values used. In the case of TpIIc_3 the new experimental data indicate that the redox-Bohr effect previously reported [22] was overestimated by approximately 15 meV per haem.

The rate constants obtained from single exponential fitting of the kinetic traces at pH 7.2 (TpIc_3) and pH 7.4 (TpIIc_3), which are a composite of the rates for individual haems, present a linear dependence on the square root of the concentration of sodium dithionite (data not shown) indicating that the reducing species for both cytochromes is SO_2^- [44]. Thus, the rate constants in Table 6 are relative to the concentration of SO_2^- which was calculated using the equilibrium constant for dissociation of sodium dithionite reported by Lambeth and Palmer [44]. Table 7 presents the values of global and weighted accessibility obtained for each cytochrome c_3 with SO_2^-. These parameters were calculated from the crystal structure (PDB code 2BQ4 and 3CAO for TpIc_3 and TpIIc_3, respectively) considering the surface accessibility of the heavy atoms of the porphyrin to a sphere of 2.5 Å. The weighted accessibility was calculated assuming that the contribution for electron transfer of the atoms of the haem substituents is reduced by a factor of 10 for each bond separating them from the macrocycle. This measure was referred to previously as the relative accessibility [30].

4. Discussion

The thermodynamic parameters obtained for both cytochromes show that the redox and acid/base centres display positive cooperativities (negative interaction energies) and that most interactions between the haems are anticooperative

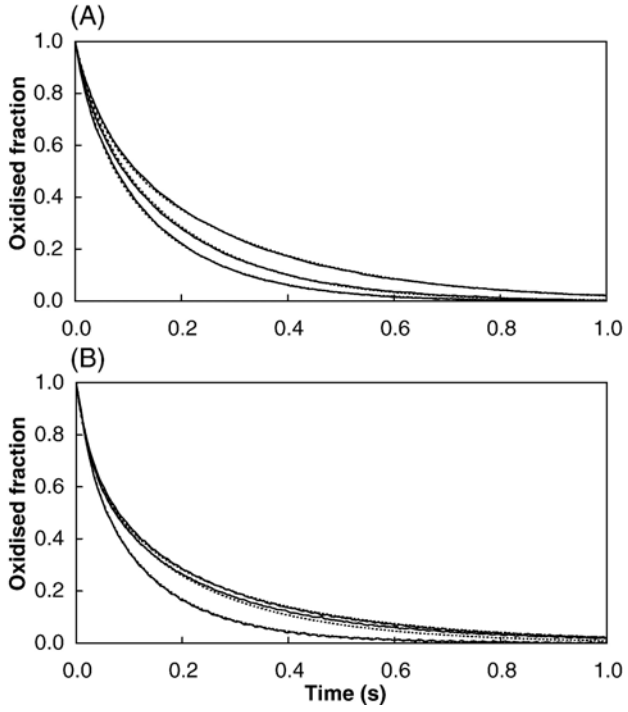

Fig. 5. Kinetics of reduction of *D. africanus* TpIc_3 and TpIIc_3 by sodium dithionite at different pH values. (A) TpIc_3 at pH 9.1 (upper trace), pH 7.2 (middle) and pH 5.7 (lower). The concentration of sodium dithionite was 270 μM and the concentration of protein was 1.14, 1.10 and 1.00 μM for the different pH, respectively. (B) TpIIc_3 at pH 8.5 (upper trace), pH 7.3 (middle) and pH 6.0 (lower). The concentration of sodium dithionite was 156 μM and the concentration of protein was 0.83, 0.75 and 0.79 μM for the different pH values, respectively. The dotted curves are the fit to the data using the parameters reported in Tables 4 and 5.

(positive interaction energies) as expected for electrostatic effects. However, the interaction energy between haems I and IV in the case of TpIc_3 and that between haems II and IV in TpIIc_3 are negative, corresponding to positive homotropic cooperativities. This can be explained by conformational changes that occur upon reduction, which may result from electrostatic reorganisation of the polypeptide chain [24,45]. In the case of TpIIc_3, a global movement of a chain fragment in the vicinity of haem III and IV that is induced by the reduction has been reported [24].

Table 4
Thermodynamic parameters determined by fitting the model to the NMR, visible and kinetic data from *D. africanus* TpIc_3 (A) and TpIIc_3 (B)

	Haem I	Haem II	Haem III	Haem IV	Ionisable centre
(A)					
Haem I	**−280** (2)	11 (2)	–	−13 (1)	−36 (1)
Haem II		**−267** (3)	–	8 (1)	−20 (1)
Haem III			**−84** (4)	–	−10 (9)
Haem IV				**−280** (2)	−26 (1)
Ionisable centre					**483** (12)
(B)					
Haem I	**−254** (2)	1 (1)	14 (2)	6 (2)	−34 (2)
Haem II		**−266** (2)	9 (1)	−8 (4)	−45 (2)
Haem III			**−265** (2)	20 (1)	−21 (2)
Haem IV				**−225** (3)	−19 (3)
Ionisable centre					**444** (4)

The fully reduced and protonated protein was taken as the reference state for all haems. Diagonal terms (in bold) are oxidation energies of the haems and deprotonation energy of the acid/base centre. Off-diagonals terms are the haem–haem and haem–proton interaction energies. All energies are reported in meV. Standard errors are given in parentheses.

Table 5
Macroscopic pK_as for the acid/base centre associated with each of the five stages of oxidation for *D. africanus* TpIc_3 and TpIIc_3

	Stage 0	Stage 1	Stage 2	Stage 3	Stage 4
TpIc_3	8.2	7.7	7.2	6.8	6.6
TpIIc_3	7.5	6.9	6.3	5.8	5.4

For TpIc_3 the order of oxidation of the haems determined from the NMR data is I–IV, II, III, whereas the order of decreasing solvent exposure is II, III, I, IV (see Table 7) which shows that solvent exposure is not the controlling factor setting the reduction potential.

Haem II in TpIc_3 presents the highest rate constant, which is in agreement with the high accessibility to the reducing agent (Table 7), and haem III presents the lowest weighted accessibility which is also in agreement with the observed rate constant. Although it is impossible to find a correlation with the two remaining haems, due to the uncertainty of the reference rate constants, it seems that the weighted accessibility may have a major contribution in controlling the kinetic rates for the case of TpIc_3, as observed for other TpIc_3 [30]. However the reference rate constants for TpIIc_3 (Table 6) do not correlate with the accessibility to the reducing agent (Table 7), indicating that the accessibility is not the only factor that controls the rates. It should be noted that reduction through collisions with SO_2^- is clearly non-physiological and, although these experiments are useful in distinguishing the properties of individual haems in the isolated proteins, the rates obtained do not refer to the electron transfer complexes.

Despite the structural similarities among the various TpIc_3, the order of reduction for their haems is different and *D. africanus* TpIc_3 shows yet a different order from that determined for other TpIc_3 characterised so far [11,30,38,39,42]. Nonetheless, *D. africanus* TpIc_3 shows positive thermodynamic cooperativity between two haems (haems I and IV) and all the haems present haem–proton interactions. These two properties appear to be the core thermodynamic features that characterise TpIc_3 cytochromes, favouring a coupled transfer of two electrons in its interaction with the periplasmic hydrogenase with electron/proton coupling that also enhances the hydrogenase activity [20].

Table 6
Reference rate constants for each haem, k_i^0, for *D. africanus* TpIc_3 and TpIIc_3

$k_i^0/10^8$ (M^{-1} s^{-1})	Haem I	Haem II	Haem III	Haem IV
TpIc_3	8.2 (4.0)	16.5 (1.1)	1.2 (0.2)	6.4 (4.0)
TpIIc_3	8.1 (0.9)	2.9 (2.7)	0.3 (4.9)	45.9 (4.0)

Standard errors with respect to an experimental error of 5% in the kinetic traces are given in parentheses.

Table 7
Global and weighted accessibility of SO_2^- to the haems of *D. africanus* TpIc_3 and TpIIc_3 in units of Å^2 (values calculated for a sphere of radius 2.5 Å (see Results)); and solvent exposure calculated for a water molecule with a sphere of radius 1.4 Å

Cytochrome			Haem I	Haem II	Haem III	Haem IV
TpIc$_3$	SO_2^-	Global	113	225	173	67
		Weighted	2.95	5.73	1.80	4.11
	H_2O	Global	196	264	222	82
TpIIc$_3$	SO_2^-	Global	204	117	117	66
		Weighted	6.62	2.54	2.24	2.66
	H_2O	Global	244	188	191	91

TpIc_3 mediates electron transfer between periplasmic hydrogenase and membrane associated redox proteins such as the high-molecular-weight cytochrome (Hmc) [15,46], the nine-haem cytochrome *c* (NhcA) [47] and the TpIIc_3 [16,19]. All these cytochromes are incorporated in multicomponent membrane complexes, suggesting the possibility of electron transfer to the quinone pool, or to the cytoplasmic reduction of sulphate, as demonstrated by growth and expression studies with wild type and mutant strains [48–51]. Thus, TpIc_3 is able to transport both electrons and protons from the bulk periplasm to the membrane surface where it is oxidised, lowering the pK_a of the protons to facilitate their release. The oxidised and deprotonated TpIc_3 can then diffuse back into the periplasm to repeat the cycle.

Preliminary titrations of TpIc_3 with TpIIc_3 followed by NMR (data not shown) are broadly in agreement with the results published in the literature [23], where it is argued that two distinct sites are preferentially used for the docking, involving haem I and II of TpIIc_3, while haem IV of TpIc_3 is mostly involved in the interaction. The assignment of the NMR signals of TpIc_3 in the present work identifies the haem methyl resonance previously reported to have the largest shift in the titration [23] as M18^1 IV. This implies a close approach between haem IV of TpIc_3 and haems I and II of TpII$_3$ which is also in agreement with the theoretical model for TpIc_3/TpIIc_3 docking complex [23,26].

Although TpIc_3 and TpIIc_3 have very similar thermodynamic parameters, as can be seen from the comparison of the redox titrations curves (Fig. 4) where the only major difference is in the reduction of the first haem, electron transfer between them is likely to occur from TpIc_3 to TpIIc_3 because the two partners must be in different redox states when they encounter each other. Hydrogenase interacts with TpIc_3 via the smaller subunit, especially around the distal and most solvent exposed [4Fe–4S] centre [52]. EPR studies showed that the [4Fe–4S] centres in [NiFe] hydrogenase have midpoint reduction potentials between −290 mV and −340 mV [53]. Therefore, hydrogenase catalyses the oxidation of H_2 (that has a midpoint potential of −413 mV at pH 7.0 and 1 atm H_2 pressure) and transfers electrons and protons to TpIc_3, which is likely to become either fully reduced or in stage 1, and protonated (see Fig. 6A). On the other hand, TpIIc_3 is probably fully oxidised (stage 4) after transferring electrons to the transmembrane complex (see Fig. 6B). The physiological partner of TpIIc_3 in *D. vulgaris* Hildenborough has been shown to be the TmcC subunit that contains two haems *b* with midpoint redox potentials of −155 and −45 mV [19]. Due to the similarity of TpIIc_3 isolated from the different organisms, it is possible that the complex in *D. africanus* with which TpIIc_3 is associated is similar to the *D. vulgaris* Hildenborough Tmc complex. In this way, a similar protein to the TmcC subunit receives electrons from TpIIc_3, and transfers them to the reduction of menaquinones, or to the reduction of sulphate.

The simplest scenario would be for TpIc_3 to encounter TpIIc_3 with TpIc_3 in the fully protonated and reduced form (stage 0) and TpIIc_3 in the fully deprotonated and oxidised state. Upon complex formation the four electrons present in TpIc_3 should equilibrate between the two cytochromes such that each of them would contain two electrons (stage 2) when the complex dissociates. The transfer of two electrons from TpIc_3 to TpIIc_3 also favours the deprotonation of TpIc_3, because the major population of stage 0 is protonated whereas in stage 2 it is less so (Fig. 6).

Upon dissociation of the complex, TpIc_3 should be deprotonated and able to react again with hydrogenase, whereas TpIIc_3 would be partially reduced and able to react with the transmembrane complex. So, based on the thermodynamic properties of the two cytochromes and on their upstream and downstream partners (hydrogenase and Tmc complex, respectively) TpIc_3 would cycle between stages 0 and 2 with the coupled movement of protons and TpIIc_3 would cycle between stages 4 and 2 without proton transfer since the major populations are deprotonated in both stages (Fig. 6).

It is certainly possible to reduce TpIc_3 under hydrogen (see Materials and methods) but the concentration of H_2 in the periplasm is probably far smaller than that used in vitro. Thus it is more likely that TpIc_3 leaves hydrogenase in stage 1. However, TpIc_3 in stage 1 would not transfer two electrons to TpIIc_3 if it is isolated from the transmembrane complex. If the encounter with TpIIc_3 occurs while it is bound to the transmembrane complex, the electrons will drain through it and leave TpIc_3 in stage 3, with a more well-defined release of protons. Since the encounter between the two cytochromes occurs near the membrane, the acidified protons are released close to the membrane surface where they can be used by the ATP synthase to power ATP phosphorylation. The transfer of a third electron from TpIc_3 to TpIIc_3 is not favoured and in this case, TpIc_3 would cycle between stages 1 and 3, transferring two electrons to TpIIc_3, which would pass the electrons to the membrane bound complex.

The complex formation between TpIc_3 and TpIIc_3 shows the dominant involvement of haem IV of TpIc_3 and haems I and II of TpIIc_3 [23,26]. Therefore faster interprotein electron transfer can be expected to involve microstates of TpIIc_3 with haem I or II oxidised given the approximate exponential dependence of electron transfer rates with distance [31,54]. Also, the electron transfer in TpIc_3 should involve microstates where haem IV is reduced, in order to be capable of electron transfer through this haem. The microscopic populations were

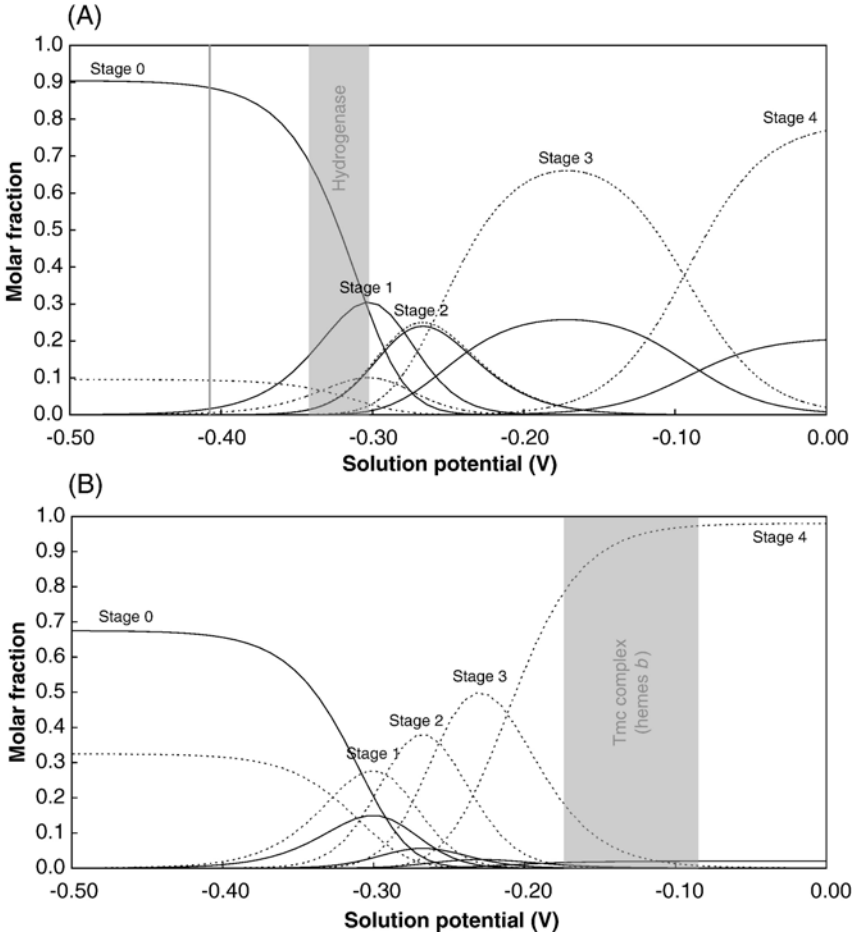

Fig. 6. Populations of the five redox oxidation stages as a function of solution potential for *D. africanus* TpIc_3 (A) and TpIIc_3 (B) at pH 7.2. The curves were calculated from the thermodynamic parameters presented in Table 4, in the protonated (solid lines) and deprotonated (dashed lines). In (A) a solid line indicates the midpoint potential of the redox H^+/H_2 pair, and a shaded bar indicates the range of reduction potentials of the Fe–S centres of hydrogenase. In (B) the shaded bar indicates the range of the reduction potentials of haems *b* in Tmc complex (see text).

calculated, for all stages, using the thermodynamic parameters for both proteins (data not shown). These populations show that, for TpIc_3 the transfer of electrons involves haem IV which is reduced in stage 1, and ready to transfer an electron. Although the dominant microstate for TpIc_3 in stage 2 has haem IV oxidised, microstates with haem IV reduced are also populated, so there is no significant energy barrier to the transfer of a second electron. In TpIIc_3, the microstates that participate in the reduction process of this cytochrome involve haems I and II, which are always free to receive electrons.

The thermodynamic characterisation of both cytochromes was made for the isolated proteins, but if the redox properties change upon complex formation, these changes are likely to facilitate electron transfer from TpIc_3 to TpIIc_3 according to theoretical docking studies [26]. Therefore the thermodynamic parameters of the two cytochromes are able to explain the electron transfer between both proteins in the physiological direction.

This is the first report of such a detailed description of the functional properties of partner proteins involved in bioenergetic metabolism containing multiple active centres. Future work will explore whether in vitro reconstitution of this section of the bioenergetic pathway upholds the current findings, or presents significant differences caused by the incorporation of TpIIc_3 in a multiprotein complex.

Acknowledgements

We would like to thank João Carita for the growth of the organisms and Isabel Pacheco for helping in the purification of the protein. Financial support was provided by contracts POCTI/QUI/47866/2002 and POCI/QUI/55690/2004 with Fundação para a Ciência e Tecnologia and fellowships to C. M. P. (SFRH/BD/6495/2001), to P.M.P (SFRH/BD/5231/2001) and to D.L.T. (SFRH/BCC/15305/2004) by Fundação para a Ciência e Tecnologia.

References

[1] J.R. Postgate, The Sulphate-Reducing Bacteria, Cambridge University Press, Cambridge, 1984.
[2] W.A. Hamilton, Microbially influenced corrosion as a model system for the study of metal microbe interactions: a unifying electron transfer hypothesis, Biofouling 19 (2003) 65–76.

[3] W.A. Hamilton, Bioenergetics of sulphate-reducing bacteria in relation to their environmental impact, Biodegradation 9 (1998) 201–212.
[4] G.R. Gibson, Physiology and ecology of the sulphate-reducing bacteria, J. Appl. Bacteriol. 69 (1990) 769–797.
[5] D.R. Lovley, Dissimilatory metal reduction, Annu. Rev. Microbiol. 47 (1993) 263–290.
[6] J.F. Heidelberg, R. Seshadri, S.A. Haveman, C.L. Hemme, I.T. Paulsen, J.F. Kolonay, J.A. Eisen, N. Ward, B. Methe, L.M. Brinkac, S.C. Daugherty, R.T. Deboy, R.J. Dodson, A.S. Durkin, R. Madupu, W.C. Nelson, S.A. Sullivan, D. Fouts, D.H. Haft, J. Selengut, J.D. Peterson, T.M. Davidsen, N. Zafar, L. Zhou, D. Radune, G. Dimitrov, M. Hance, K. Tran, H. Khouri, J. Gill, T.R. Utterback, T.V. Feldblyum, J.D. Wall, G. Voordouw, C.M. Fraser, The genome sequence of the anaerobic, sulfate-reducing bacterium *Desulfovibrio vulgaris* Hildenborough, Nat. Biotechnol. 22 (2004) 554–559.
[7] J. Le Gall, W.J. Payne, L. Chen, M.Y. Liu, A.V. Xavier, Localization and specificity of cytochromes and other electron transfer proteins from sulfate-reducing bacteria, Biochimie 76 (1994) 655–665.
[8] P.M. Matias, I.A. Pereira, C.M. Soares, M.A. Carrondo, Sulphate respiration from hydrogen in *Desulfovibrio* bacteria: a structural biology overview, Prog. Biophys. Mol. Biol. 89 (2005) 292–329.
[9] R.O. Louro, Proton thrusters: overview of the structural and functional features of soluble tetrahaem cytochromes *c*3, J. Biol. Inorg. Chem. 12 (2007) 1–10.
[10] M. Coletta, T. Catarino, J. LeGall, A.V. Xavier, A thermodynamic model for the cooperative functional properties of the tetraheme cytochrome c_3 from *Desulfovibrio gigas*, Eur. J. Biochem. 202 (1991) 1101–1106.
[11] D.L. Turner, C.A. Salgueiro, T. Catarino, J. LeGall, A.V. Xavier, NMR studies of cooperativity in the tetrahaem cytochrome c_3 from *Desulfovibrio vulgaris*, Eur. J. Biochem. 241 (1996) 723–731.
[12] H. Santos, J.J.G. Moura, I. Moura, J. LeGall, A.V. Xavier, NMR studies of electron transfer mechanisms in a protein with interacting redox centres: *Desulfovibrio gigas* cytochrome c_3, Eur. J. Biochem. 141 (1984) 283–296.
[13] R.O. Louro, I. Pacheco, D.L. Turner, J. LeGall, A.V. Xavier, Structural and functional characterization of cytochrome c_3 from *D. desulfuricans* ATCC 27774 by ^{1}H-NMR, FEBS Lett. 390 (1996) 59–62.
[14] V. Magro, L. Pieulle, N. Forget, B. Guigliarelli, Y. Petillot, E.C. Hatchikian, Further characterization of the two tetraheme cytochromes c_3 from *Desulfovibrio africanus*: nucleotide sequences, EPR spectroscopy and biological activity, Biochim. Biophys. Acta 1342 (1997) 149–163.
[15] I.A.C. Pereira, C.V. Romão, A.V. Xavier, J. LeGall, M. Teixeira, Electron transfer between hydrogenases and mono- and multiheme cytochromes in *Desulfovibrio* ssp, J. Biol. Inorg. Chem. 3 (1998) 494–498.
[16] F.M.A. Valente, L.M. Saraiva, J. LeGall, A.V. Xavier, M. Teixeira, I.A.C. Pereira, A membrane-bound cytochrome c_3: a Type II cytochrome c3 from *Desulfovibrio vulgaris* Hildenborough, ChemBioChem 2 (2001) 895–905.
[17] P.M. Matias, L.M. Saraiva, C.M. Soares, A.V. Coelho, J. LeGall, M.A. Carrondo, Nine-haem cytochrome *c* from *Desulfovibrio desulfuricans* ATCC 27774: primary sequence determination, crystallographic refinement at 1.8 and modelling studies of its interaction with the tetrahaem cytochrome c_3, J. Biol. Inorg. Chem. 4 (1999) 478–494.
[18] C. Aubert, M. Brugna, A. Dolla, M. Bruschi, M.T. Giudici-Orticoni, A sequential electron transfer from hydrogenases to cytochromes in sulphate-reducing bacteria, Biochim. Biophys. Acta 1476 (2000) 85–92.
[19] P.M. Pereira, M. Teixeira, A.V. Xavier, R.O. Louro, I.A. Pereira, The Tmc complex from *Desulfovibrio vulgaris* Hildenborough is involved in transmembrane electron transfer from periplasmic hydrogen oxidation, Biochemistry 45 (2006) 10359–10367.
[20] R.O. Louro, T. Catarino, J. LeGall, A.V. Xavier, Redox-Bohr effect in electron/proton energy transduction: cytochrome c_3 coupled to hydrogenase works as a 'proton thruster' in *Desulfovibrio vulgaris*, J. Biol. Inorg. Chem. 2 (1997) 488–491.
[21] R.O. Louro, T. Catarino, D.L. Turner, M.A. Picarra-Pereira, I. Pacheco, J. LeGall, A.V. Xavier, Functional and mechanistic studies of cytochrome c_3 from *Desulfovibrio gigas*: thermodynamics of a "proton thruster", Biochemistry 37 (1998) 15808–15815.
[22] P.M. Pereira, I. Pacheco, D.L. Turner, R.O. Louro, Structure–function relationship in type II cytochrome c_3 from *Desulfovibrio africanus*: a novel function in a familiar heme core, J. Biol. Inorg. Chem. 7 (2002) 815–822.
[23] L. Pieulle, X. Morelli, P. Gallice, E. Lojou, P. Barbier, M. Czjzek, P. Bianco, F. Guerlesquin, E.C. Hatchikian, The type I/type II cytochrome c_3 complex: an electron transfer link in the hydrogen-sulfate reduction pathway, J. Mol. Biol. 354 (2005) 73–90.
[24] S. Norager, P. Legrand, L. Pieulle, C. Hatchikian, M. Roth, Crystal structure of the oxidised and reduced acidic cytochrome c_3 from *Desulfovibrio africanus*, J. Mol. Biol. 290 (1999) 881–902.
[25] L. Pieulle, J. Haladjian, J. Bonicel, E.C. Hatchikian, Biochemical studies of the c-type cytochromes of the sulfate reducer *Desulfovibrio africanus*. Characterization of two tetraheme cytochromes c_3 with different specificity, Biochim. Biophys. Acta 1273 (1996) 51–61.
[26] V.H. Teixeira, A.M. Baptista, C.M. Soares, Modeling electron transfer thermodynamics in protein complexes: interaction between two cytochromes c_3, Biophys. J. 86 (2004) 2773–2785.
[27] C.A. Salgueiro, D.L. Turner, H. Santos, J. LeGall, A.V. Xavier, Assignment of the redox potentials to the four haems in *Desulfovibrio vulgaris* cytochrome c_3 by 2D-NMR, FEBS 314 (1992) 155–158.
[28] R. Pierattelli, L. Banci, D.L. Turner, Indirect determination of magnetic susceptibility tensors in peroxidases: a novel approach to structure elucidation by NMR, J. Biol. Inorg. Chem. 1 (1996) 320–329.
[29] R.L.J. Keller, The Computer Aided Resonance Assignment Tutorial 1st edn., CANTINA Verlag 3-85600-112-3, 2004.
[30] I.J. Correia, C.M. Paquete, A. Coelho, C.C. Almeida, T. Catarino, R.O. Louro, C. Frazão, L.M. Saraiva, M.A. Carrondo, D.L. Turner, A.V. Xavier, Proton-assisted two-electron transfer in natural variants of tetraheme cytochromes from *Desulfomicrobium* sp. J. Biol. Chem. 279 (2004) 52227–52237.
[31] P.L. Dutton, Redox potentiometry: determination of midpoint potentials of oxidation–reduction components of biological electron-transfer systems, Methods Enzymol. 54 (1978) 411–435.
[32] M. Dixon, The acceptor specificity of flavins and flavoproteins. I. Techniques for anaerobic spectrophotometry, Biochim. Biophys. Acta 226 (1971) 241–258.
[33] T. Catarino, D.L. Turner, Thermodynamic control of electron transfer rates in multicentre redox proteins, ChemBioChem 2 (2001) 416–424.
[34] D.L. Turner, C.A. Salgueiro, J. LeGall, A.V. Xavier, Structural studies of *Desulfovibrio vulgaris* ferrocytochrome c_3 by two-dimensional NMR, Eur. J. Biochem. 210 (1992) 931–936.
[35] M. Pessanha, L. Brennan, A.V. Xavier, P.M. Cuthbertson, G.A. Reid, S.K. Chapman, D.L. Turner, C.A. Salgueiro, NMR structure of the haem core of a novel tetrahaem cytochrome isolated from *Shewanella frigidimarina*: identification of the haem-specific axial ligands and order of oxidation, FEBS Lett. 489 (2001) 8–13.
[36] G.P. Moss, Nomenclature of tetrapyrroles. Recommendations 1986 IUPAC-IUB Joint Commission on Biochemical Nomenclature (JCBN), Eur. J. Biochem. 178 (1988) 277–328.
[37] C.A. Salgueiro, D.L. Turner, A.V. Xavier, Use of paramagnetic NMR probes for structural analysis in cytochrome c_3 from *Desulfovibrio vulgaris*, Eur. J. Biochem. 244 (1997) 721–734.
[38] J.S. Park, T. Ohmura, K. Kano, T. Sagara, K. Niki, Y. Kyogoku, H. Akutsu, Regulation of the redox order of four hemes by pH in cytochrome c_3 from *D. vulgaris* Miyazaki F, Biochim. Biophys. Acta 1293 (1996) 45–54.
[39] R.O. Louro, I.J. Correia, L. Brennan, I.B. Coutinho, A.V. Xavier, D.L. Turner, Electronic structure of low-spin ferric porphyrins: C-13 NMR studies of the influence of axial ligand orientation, J. Am. Chem. Soc. 120 (1998) 13240–13247.
[40] D.L. Turner, C.A. Salgueiro, P. Schenkels, J. LeGall, A.V. Xavier, Carbon-13 NMR studies of the influence of axial ligand orientation on haem electronic structure, Biochim. Biophys. Acta 1246 (1995) 24–28.
[41] I. Moura, M. Teixeira, B.H. Huynh, J. LeGall, J.J. Moura, Assignment of individual heme EPR signals of *Desulfovibrio baculatus* (strain 9974) tetraheme cytochrome c_3. A redox equilibria study, Eur. J. Biochem. 176 (1988) 365–369.
[42] R.O. Louro, T. Catarino, J. LeGall, D.L. Turner, A.V. Xavier, Cooperativity between electrons and protons in a monomeric cytochrome

c_3: the importance of mechano-chemical coupling for energy transduction, ChemBioChem 2 (2001) 831–837.
[43] T. Ohmura, H. Nakamura, K. Niki, M.A. Cusanovich, H. Akutsu, Ionic strength-dependent physicochemical factors in cytochrome c_3 regulating the electron transfer rate, Biophys. J. 75 (1998) 1483–1490.
[44] D.O. Lambeth, G. Palmer, The kinetics and mechanism of reduction of electron transfer proteins and other compounds of biological interest by dithionite, J. Biol. Chem. 248 (1973) 6095–6103.
[45] R.O. Louro, T. Catarino, C.M. Paquete, D.L. Turner, Distance dependence of interactions between charged centres in proteins with common structural features, FEBS Lett. 576 (2004) 77–80.
[46] M. Rossi, W.B. Pollock, M.W. Reij, R.G. Keon, R. Fu, G. Voordouw, The *hmc* operon of *Desulfovibrio vulgaris* subsp. *vulgaris* Hildenborough encodes a potential transmembrane redox protein complex, J. Bacteriol. 175 (1993) 4699–4711.
[47] P.M. Matias, R. Coelho, I.A.C. Pereira, A.V. Coelho, A.W. Thompson, L.C. Sieker, J. Le Gall, M.A. Carrondo, The primary and three-dimensional structures of a nine-haem cytochrome *c* from *Desulfovibrio desulfuricans* ATCC 27774 reveal a new member of the Hmc family, Structure 7 (1999) 119–130.
[48] S.A. Haveman, V. Brunelle, J.K. Voordouw, G. Voordouw, J.F. Heidelberg, R. Rabus, Gene expression analysis of energy metabolism mutants of *Desulfovibrio vulgaris* Hildenborough indicates an important role for alcohol dehydrogenase, J. Bacteriol. 185 (2003) 4345–4353.
[49] J.L. Steger, C. Vincent, J.D. Ballard, L.R. Krumholz, *Desulfovibrio* sp. genes involved in the respiration of sulfate during metabolism of hydrogen and lactate, Appl. Environ. Microbiol. 68 (2002) 1932–1937.
[50] R.G. Keon, R. Fu, G. Voordouw, Deletion of two downstream genes alters expression of the *hmc* operon of *Desulfovibrio vulgaris* subsp. *vulgaris* Hildenborough, Arch. Microbiol. 167 (1997) 376–383.
[51] A. Dolla, B.K. Pohorelic, J.K. Voordouw, G. Voordouw, Deletion of the *hmc* operon of *Desulfovibrio vulgaris* subsp. *vulgaris* Hildenborough hampers hydrogen metabolism and low-redox-potential niche establishment, Arch. Microbiol. 174 (2000) 143–151.
[52] P.M. Matias, C.M. Soares, L.M. Saraiva, R. Coelho, J. Morais, J. Le Gall, M.A. Carrondo, [NiFe] hydrogenase from *Desulfovibrio desulfuricans* ATCC 27774: gene sequencing, three-dimensional structure determination and refinement at 1.8 A and modelling studies of its interaction with the tetrahaem cytochrome c_3, J. Biol. Inorg. Chem. 6 (2001) 63–81.
[53] M. Teixeira, I. Moura, A.V. Xavier, J.J.G. Moura, J. Legall, D.V. Dervartanian, H.D. Peck, B.H. Huynh, Redox intermediates of *Desulfovibrio gigas* [Nife] Hydrogenase generated under hydrogen — Mossbauer and EPR characterization of the metal centers, J. Biol. Chem. 264 (1989) 16435–16450.
[54] H.B. Gray, J.R. Winkler, Electron tunneling through proteins, Q. Rev. Biophys. 36 (2003) 341–372.